

Chemodynamics analysis in the galaxy Haro 15

Verónica Firpo^{1,2}*, Guillermo Hägele^{1,2,3}, Guillermo Bosch^{1,2}, Ángeles I. Díaz³, Nidia Morrell⁴

1 - Facultad de Ciencias Astronómicas y Geofísicas, Universidad Nacional de La Plata, Argentina. 2 - IALP - CONICET, Argentina
3 - Departamento de Física Teórica, C-XI, Universidad Autónoma de Madrid, Spain. 4 - Las Campanas Observatory, Carnegie Observatories, La Serena, Chile.

ABSTRACT

We present a detailed study of the physical properties of the nebular material in four star-forming knots of the galaxy Haro 15. Using long-slit and echelle spectroscopy obtained at Las Campanas Observatory, we study the physical conditions (electron density and temperatures), ionic and total chemical abundances of several atoms, reddening and ionization structure, for the global flux and for the different kinematical components. The latter was derived by comparing the oxygen and sulphur ionic ratios to their corresponding observed emission line ratios (the η and η' plots) in different regions of the galaxy. Applying the direct method or empirical relationships for abundance determination, we perform a comparative analysis between these regions. The similarities found in the ionization structure of the different kinematical components implies that the effective temperatures of the ionizing radiation fields are very similar in spite of some small differences in the ionization state of the different elements. Therefore the different gaseous kinematical components identified in each star-forming knot are probably ionized by the same star cluster. However, the difference in the ionizing structure of the two knots with knot A showing a lower effective temperature than knot B, suggests a different evolutionary stage for them consistent with the presence of an older and more evolved stellar population in the first. This is the first time that physical conditions are directly estimated for kinematical components of HII galaxies.

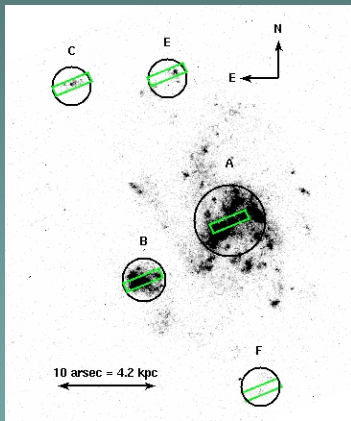


Figure 1: Finding chart for the regions observed in Haro 15, identified by circles and labeled following Caróns et al. (2001). Green rectangles show the positions of echelle slit. Wide Field Planetary Camera 2 H α image was obtained from the Multimission Archive at the Space Telescope Science Institute (MAST).

OBSERVATIONS

We obtained high resolution spectroscopy (Echelle Spectrograf, the spectral resolution is R 25000: $\Delta\lambda = 0.25\text{\AA}$ at 6000 \AA , equivalent to velocity resolution of 12 km s⁻¹) and long-slit moderate resolution spectroscopy (WFCCD; the spectral resolution is R 900: $\Delta\lambda = 7.5\text{\AA}$ at 6700 \AA) of four and two luminous knots, respectively, in the galaxy Haro 15 at the du Pont Telescope, in July 2006 and September 2005, respectively. Observing conditions were good, with an average seeing of 1" and photometric nights. Spectrophotometric standards, according to the respective observing mode, were also observed.

Our obtained results are plotted together with the WHT objects from Hägele et al. (2006) and CAHA objects from Hägele et al. (2008), and HII galaxies from the literature listed in Hägele et al. (2008).

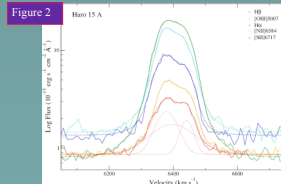


Figure 2

INTERNAL KINEMATIC

The two brightest star-forming knots A and B show, in our high spectral resolution spectra, complex structure which, although evident in radial velocity space, could not be spatially resolved. All Haro 15 emission knots show evidence of wing broadening evident mainly in the H α line and confirmed in other emission lines.

Following the iterative procedure presented in Firpo et al. (2010), we measured the fluxes associated with each kinematical component identified in the high resolution echelle data for the strongest emission lines. The validity of the profile multiplicity and broadening is checked over the different emission lines, becoming more evident in the strong H α emission line.

Figure 2 (Firpo et al., 2011) is an example of the good correlation found between the emission line profiles in the Log Flux-Velocity plane of the most intense emission lines in Knot A and shows the multiple gaussian fit to the H α emission line in this knot. The Gaussian fits in Knot A reveal the presence of two distinctly separated kinematical components with a velocity dispersion of about 25 km/s in each one. In Knot B there seems to be more than one component, but it is only possible to fit a single Gaussian component with a velocity dispersion of 20 km/s. The profile fittings show the presence of a residual in the emission line wings in both knots. We are able to fit a broad component, with a velocity dispersion of about 67 km/s in the Knot A and 40 km/s in Knot B.

For those lines with S/N too low to perform a self-consistent fitting of the different kinematical components present in their emission profiles, the iterative process used to deconvolve the different components did not yield meaningful results. For these weak emission lines we used the fitting found for the strongest emission lines with similar ionization degree as the initial guess. With these we fit the emission profiles of the weak lines fixing the centroids and widths of the corresponding initial approximation, allowing only the profiles amplitudes to vary.

ELECTRON DENSITY AND TEMPERATURES

The different methods used to estimate the electron temperatures (T_e) and densities [$N_e \approx n(\text{S II})$] are described in detail in Hägele et al. (2012), and references therein). The analysis was done on the global measurements performed to the emission lines of the spectra obtained with both instruments, and on the different kinematical components deconvolved in the emission line profiles in the high resolution data.

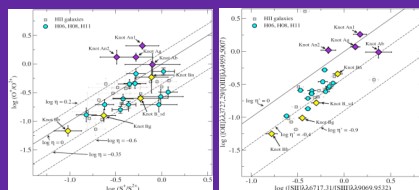
For all observed knots, and for all the global measurements and kinematical components, the Ne were found to be well below the critical density for collisional de-excitation, as is well known to occur in the star-forming processes belonging to HII galaxies. Only for the global measure in the case of Knot B observed with the long-slit spectrograph, we obtained an electron density with good accuracy, 150=50 particles per cm³.

From the simple dispersion spectra, in Knot B we measured four line temperatures: $T_e(\text{OIII})$, $T_e(\text{OII})$, $T_e(\text{SIII})$ and $T_e(\text{SII})$ reaching high precision, with rms fractional errors of the order of 2%, 3%, 10% and 14%, respectively. We estimated $T_e(\text{NII})$ considering the approximation $T_e(\text{NII}) = T_e(\text{OII})$. We found that $T_e(\text{OII})$ in this knot is 4100K higher than $T_e(\text{SII})$ instead of a similar value as it is predicted by the models. For Knot C, from model based and empirical temperature relations, we estimated: $T_e(\text{OIII})$, $T_e(\text{OII})$, $T_e(\text{SIII})$, $T_e(\text{SII})$ and $T_e(\text{NII})$.

From the echelle spectra of Knot B, for the global measure and for the two kinematical components, we measured $T_e(\text{OIII})$ and $T_e(\text{SIII})$ applying the direct method. We have reached high precision from the global measure and the broad component for the first temperature, with rms fractional errors of the order of 5 and 4 %, respectively, and slightly worse, 15 % for the narrow component. We have also obtained good precision for the estimates of the $T_e(\text{SIII})$, 13, 18, and 14 % from the global measure, the narrow and the broad components, respectively.

This is the first time for this kind of star-forming galaxies than the auroral emission lines needed to apply the direct method to calculate the line temperatures have been decomposed in their kinematical components. This fact allows us to estimate the T_e of the emitting gas that originate each component present in the emission line profiles. The $T_e(\text{OII})$ was obtained from model based relationships, and $T_e(\text{SII})$ and $T_e(\text{NII})$ were assumed equal to $T_e(\text{OII})$. For the other star-forming knots, A, C, and E, the T_e are estimated using model based and empirical temperature relationships, depending on the available emission lines for each case.

IONIZATION STRUCTURE



The right panel shows the purely observational counterpart of the left panel. The diagonal lines represent constant values of $\log \eta'$ defined by Vilchez & Pagel (1988) as:

$$\log \eta' = \log \left(\frac{[\text{OIII}]/[\text{OII}]}{([\text{SII}]/[\text{SIII}])} \right)$$

Where η and η' are related through the electron temperature but very weakly.

The ionization structure of knots A and B shows very similar values within the errors for the different components of each of these regions. Only the broad component of knot A seems to have slightly higher effective temperature than the other components. These similarities imply that the effective temperatures of the ionizing radiation fields are very similar for all the different kinematical components. The ionizing star clusters that excite the gas belonging to each star-forming knot that produces the different kinematical components could therefore be the same. The difference in the ionization structure of these two knots suggests a different evolutionary stage, with knot A located in a region with lower effective temperature than that where knot B is placed. This is in agreement with the presence of an older and more evolved stellar population in knot A than in knot B, as suggested by López-Sánchez & Esteban (2010).

The ratio between O^+/O^{2+} and S^+/S^{2+} denoted by η is intrinsically related to the shape of the ionizing continuum and depends on nebula geometry only slightly (Vilchez & Pagel, 1988). In the left panel is shown the relation between $\log(\text{O}^+/\text{O}^{2+})$ and $\log(\text{S}^+/\text{S}^{2+})$. Diagonal lines corresponds to constant values of η . The HII galaxies and HII regions occupy the central region which corresponds to high values of the ionizing temperature. We include knot A and B (filled violet and yellow diamonds, respectively). The letter added to the name of each knot denotes the instrument (for the long-slit spectrum) or the components (for echelle data).

SUMMARY

From low and high resolution spectroscopy we have analyzed five star forming knots in the Haro15 galaxy. The $[\text{OIII}]\lambda 4363\text{\AA}$ emission line is only detected in knot B. We are able to obtain a direct estimation of $T(\text{OIII})$ and $T(\text{SIII})$ for the global measurements and different kinematical components, and performed the direct chemodynamics calculation for two ionic abundances, O^{2+} and S^{2+} . This is the first time for this kind of star-forming galaxies than the auroral emission lines needed to apply the direct method to calculate the line temperatures have been decomposed in their kinematical components. The O/H derived for knot B is in very good agreement with the value estimated by López-Sánchez & Esteban (2009). For knots A and B, the relative abundances of N/O, S/O, Ne/O and Ar/O for the different kinematical components are very similar; these could be evidence for a common or very similar chemical evolution for the different kinematical components of each knot. It could also be indicative that the different kinematical components are different phases of the same gas. Our results from ionization structure to chemical abundances support these differences between the two knots. The difference in the ionizing structure of these two knots suggests a different evolutionary stage.

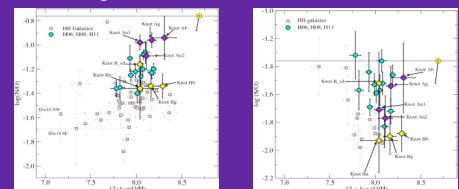
OXYGEN ABUNDANCES

Oxygen abundances and their uncertainties were derived for each observed knot. Using the estimated values for the Ne and Te and a careful and realistic treatment of observational errors, we have estimated ionic and total abundances of O, S, N, Ne, Ar, Fe and He, depending on the available emission lines for each star-forming knot. For the echelle spectroscopy data, we have been able to carry out a chemodynamics analysis from the kinematical component decomposition of the emission line profiles.

In Knot B, for which we could calculate two line temperatures using the direct method, we have performed the direct chemodynamics calculation for two ionic abundances, O^{2+} and S^{2+} , this kind of analysis had never been done until now for this type of objects.

The obtained total abundances of O, S, N, Ne, and Ar are in the typical range found for HII galaxies. The total oxygen abundance derived for knot B is in very good agreement with the value estimated by López-Sánchez & Esteban (2009). The total oxygen abundance derived for all the measurements of the echelle data of this knot are in good agreement with the global measure being approximately the average of the derived values for the different kinematical components weighted by luminosity. For knot A, the derived total oxygen abundance from the global measure is lower (-0.2 dex) than the value found by López-Sánchez & Esteban (2009).

Total oxygen abundances derived for knots A, B, C, and E are very similar among themselves considering the observational errors.



We show N/O and S/O as a function of $12+\log(\text{O}/\text{H})$ (left- and right-hand panel, respectively) for knots A and B (open and filled diamonds, violet and yellow, respectively). The observed knots are marked in the plot with their names plus a letter which denote the observation mode ('sd': single dispersion) or the kinematical component measure ('g': global, 'n': narrow and 'b': broad). The ionic abundances are shown with the usual sun symbol: oxygen from Allende Prieto et al. (2001), nitrogen from Holweger (2001) and sulphur from Grevesse & Sauval (1998). These values are linked by a solid line with the solar ratios from Asplund et al. (2005).

References

- Firpo et al., 2010, Mon. Not. R. Astron. Soc., 406, 1094
- Firpo et al., 2011, Mon. Not. R. Astron. Soc., 414, 3288
- Hägele et al., 2006, Mon. Not. R. Astron. Soc., 372, 293
- Hägele et al., 2008, Mon. Not. R. Astron. Soc., 383, 209
- Hägele et al., 2011, Mon. Not. R. Astron. Soc., 414, 272
- Hägele et al., 2012, Mon. Not. R. Astron. Soc., 422, 3478
- Isotov et al., 1994, AJP, 435, 667
- Isotov et al., 2006, A&A, 448, 955
- López-Sánchez A. R., Esteban C., 2009, A&A, 508, 615
- López-Sánchez A. R., Esteban C., 2010, A&A, 517, A85
- Pagel B. E. J., et al., 1992, Mon. Not. R. Astron. Soc., 255, 325
- Pérez-Montero E., Díaz A. I., 2003, Mon. Not. R. Astron. Soc., 346, 1063
- Hägele et al., 2008, Mon. Not. R. Astron. Soc., 383, 209
- Pérez-Montero E., et al., 2007, Mon. Not. R. Astron. Soc., 381, 125
- Stammler G., 1990, Astron. and Astrophys. Suppl. Series, 83, 501
- Vilchez J. M., Pagel B. E. J., 1988, Mon. Not. R. Astron. Soc., 231, 257
- Vilchez J. M., Esteban C., 1996, Mon. Not. R. Astron. Soc., 280, 720